Decentralized Blockchain Based Dynamic Spectrum Acquisition for Wireless Downlink Communications

Miao Jiang, Yiqing Li, Qi Zhang, *Member*, *IEEE*, and Jiayin Qin

***Abstract*—Wireless network virtualization is a promising solution to improve the spectrum efficiency. For a wireless downlink communication system with multiple mobile virtual network operators (MVNOs), we propose a decentralized blockchain based dynamic spectrum acquisition scheme. Our proposed scheme aims to minimize the sum transmit power at all MVNOs while satisfying the average data transmission rate thresholds. For each MVNO, the required wireless spectrum to provide customized services to the mobile users (MUs) is predicted using the half-range Gauss-Hermite quadrature. Based on the predicted values, all the MVNOs carry out a blockchain-based distributed alternative direction method of multipliers to obtain the global optimal solution to the aforementioned sum transmit power minimization problem. To examine the effectiveness of our proposed scheme, with known system parameters, we also theoretically derive the semi-closed-form solution to the actually required sum transmit power minimization problem subject to data transmission rate constraints. Simulation results illustrate that our proposed dynamic spectrum acquisition scheme achieves almost the same minimum sum power as the non-causal scheme which assumes the number of active MUs in all cells and all the channels are known non-causally for the optimal dynamic spectrum allocation.**

***Index Terms*—Alternating direction method of multipliers (ADMM), blockchain, dynamic spectrum acquisition, wireless network virtualization.**

I. Introduction

With the popularity of various smartphones, an exponential traffic growth is generated by wireless applications in next generation 5G networks and beyond [1]–[4]. To cope with the dramatic traffic growth, network densification is expected to increase by 1000 times ranging from macrocells to femtocells [5]. Thus, a serious spectrum shortage problem should be properly addressed. To solve the spectrum shortage problem, either we release more licensed bandwidth for next generation 5G networks and beyond, or we improve the spectrum efficiency by employing the efficient spectrum management schemes.

To improve the spectrum efficiency, wireless network virtualization is a promising solution [6]–[8]. Wireless network virtualization is able to facilitate multiple network operators to share common resources, e.g., licensed spectrum. The virtualized wireless networks (VWNs) commonly consist of multiple mobile network operators (MNOs) and multiple mobile virtual network operators (MVNOs) [9]. The MNO owns the physical cellular infrastructure and radio resources, it executes the virtualization by leasing the isolated virtualized network resources to the MVNO. The MVNO leases the resources from the MNO and then assigns the resources to the MUs. The spectrum resources which belong to one or more MNOs are virtualized and split into slices. The MVNO utilizes the slices leased from MNOs depending on the quality-of-service (QoS) of MUs. Recently, wireless network virtualization had attracted an increasing attention from the research community [10]–[13]. In [10], an active sharing of physical infrastructure and the spectrum was proposed, where MNOs share the network resources and provide wholesale access to MVNOs, allowing them to provide voice and data services using part of the available resources. The work in [11] introduced a novel scheme for slicing and scheduling for VWNs by developing an efficient resource allocation scheme. In [12], an efficient low-complexity scheme was put forward to virtualize the wireless resource blocks and share them between MUs of multiple MNOs. The scheme aims to maximize the throughput while maintaining access proportional fairness among MUs as well as MNOs. In [13], a two-stage spectrum leasing problem with the goal of maximizing the average profit of a MVNO was investigated.

Aforementioned dynamic spectrum allocation schemes in VWNs improve the spectrum efficiency in a centralized manner which requires a central node. If the central node is under cyberattack, all the MVNOs are vulnerable. In addition, if the MVNOs belong to different MNOs, the information exchange among different nodes should be as less as possible. Furthermore, the management overhead increases with the increase of the number of MVNOs which causes that the wireless communication system is not scalable. Therefore, in this paper, we propose a decentralized blockchain based dynamic spectrum acquisition scheme.

Blockchain, which was invented by Satoshi Nakamoto in 2008, is an emerging technology to build consensus between disparate individuals [14]. The intuition is to solve the double-spending problem in the cryptocurrency Bitcoin without the use of a trusted central utility. Blockchain consists of lists of blocks which are linked by the hash algorithm. Each block includes collections of signatured transactions. A new block can be appended to the end of the current blockchain after solving a proof-of-work (PoW) puzzle which is to find a number whose hash value is less than the current target. PoW can create distributed consensus between all participants and solve the double-spending problem. The data on blockchain is shared and saved by all participants on peer-to-peer networks. All participants have right to access but cannot tamper the

M. Jiang, Y. Li, and Q. Zhang are with the School of Electronics and Information Technology, Sun Yat-sen University, Guangzhou 510006, Guangdong, China (e-mail: jmiao@mail2.sysu.edu.cn, liyiq5@mail2.sysu.edu.cn, zhqi26@mail.sysu.edu.cn). J. Qin is with the School of Electronics and Information Technology, Sun Yat-sen University, Guangzhou 510006, Guangdong, China, and also with the Xinhua College, Sun Yat-sen University, Guangzhou 510520, Guangdong, China (e-mail: issqjy@mail.sysu.edu.cn).

data on blockchain. The pillars of blockchain are state-of-the-art cryptography and PoW based distributed consensus mechanism. This kind of system may introduce some computational cost but can provide decentrality, security, transparency and robustness. The blockchain technologies have been extensively used in many areas [15]–[20].

In the Bitcoin system, users are only allowed to perform a set of given operations. Due to this non-Turing-completeness, it cannot handle more complex business logic. In order to solve this problem, Ethereum was proposed by Vitalik Buterin in 2013 [21]. Ethereum is a Turing-complete system where users can develop programs to run on the Ethereum virtual machine using high-level programming languages. These programs, also called as smart contracts [22], will work automatically and transparently with pre-coded logic once deployed. The correct execution of smart contracts can be ensured by the consensus mechanism when the reliable nodes are the majority in the network [21].

Both Bitcoin and Ethereum belong to public blockchains [23]. Public blockchains, sometimes referred to as permissionless blockchains, are totally decentralized blockchains that open to everyone in the world. Everyone can take participant in the public blockchains from everywhere at any time without registration and authentication. Everyone has right to operate the blockchains, such as sending and verifying new transactions as well as reading and saving past verified transactions.

In public blockchains, the consensus is built between all participants with Nakamoto-type incentive mechanism, such as PoW and proof of stake [24] protocol. In order to stimulate nodes to help maintain the blockchain instead of attacking and subverting, cryptocurrency is awarded to the consensus participants according to their computational effort. Due to a large number of participants, achieving consensus in public blockchains is time-consuming and power-demanding which restricts the application of blockchains in many scenarios.

Besides public blockchains, another primary type of blockchains is permissoned blockchains [25]. Permissoned blockchains are also called as private blockchains or consortium blockchains when they are managed by one or more predefined participants respectively. In permissioned blockchains, permissions to join and operate the blockchains are strictly controlled by predefined participants. Predefined participants are responsible for creating consensus in permissoned blockchains.

Due to the limited number of predefined participants and controllable trust between them, more efficient electing and voting based low complexity consensus algorithm can be employed. For example, practical Byzantine fault tolerance (PBFT) [26] based three rounds double-check protocol is adopted by HyperLedger Fabric v0.5 [27]. Both Raft [28] and PBFT-inspired consensus algorithms are employed by Quorum [29] and R3 Corda [30]. Compared with the throughput of dozens transactions per second (TPS) in public blockchains, private blockchains can handle approximately thousands TPS [31] which can meet the demand in most application scenarios.

In this paper, we propose a decentralized blockchain based dynamic spectrum acquisition scheme for a wireless downlink communication system with multiple MVNOs. With wireless network virtualization operation, the whole communication processes are divided into multiple periods, each measured in minutes. At the beginning of each period, MVNOs should predict the required wireless spectrum to provide customized services to the MUs in their respective service cells. Based on the predicted values, MVNOs acquire wireless spectrum by our proposed decentralized blockchain based dynamic spectrum acquisition scheme. Our proposed scheme aims to minimize the sum transmit power at all MVNOs while satisfying the average data transmission rate thresholds. We propose to employ the half-range Gauss-Hermite quadrature (HR-GHQ) to simplify the optimization problem. Then, we propose a blockchain-based distributed alternative direction method of multipliers (ADMM) to obtain the global optimal solution to aforementioned sum transmit power minimization problem.

To fairly compare the performance of our proposed scheme with the fixed spectrum allocation scheme and other schemes, with known system parameters, we propose to investigate the actually required minimum sum transmit power of all MVNOs subject to that the data transmission rate thresholds for all MUs in all cells are satisfied. We theoretically derive semi-closed-form expressions for the optimal power and spectrum allocation for each MVNO.

The remainder of the paper is organized as follows. The system model and dynamic spectrum acquisition optimization problem formulation are described in Section II and Section III, respectively. We propose the blockchain based distributed ADMM algorithm for dynamic spectrum acquisition in Section IV. With known system parameters, the optimal power and spectrum allocation is theoretically derived in Section V. Section VI provides simulation results to validate the effectiveness of our proposed scheme. Section VII concludes this paper.

Notations: Boldface lowercase letters denote vectors. $(\cdot)^T$ denotes the transpose operation. $\|\cdot\|_1$ and $\|\cdot\|_2$ represent the l_1 and l_2 norm of a vector, respectively.

II. System Model

Consider a wireless downlink communication system with M MVNOs. It is assumed that most of MVNOs are reliable. They are predefined participants of a permissioned blockchain regulated by MNO. Smart contract can be deployed on the blockchain to help MNO manager the network. MNO controls who is reliable to join the blockchain and kicks out who intends to do evil. MNO also bills the MVNOs and authorizes them to use the spectrum with the help of smart contracts. All MVNOs have permissions to operate the blockchain. The consensus is built by all MVNOs via low complexity consensus algorithm, e.g. PBFT and Raft. Each MVNO serves the MUs in a cell. The m-th transmission cell, $m \in \mathcal{M} = \{1, 2, \cdots, M\}$, is assumed to be a fixed circular region, denoted as $\mathcal{D}_m \in \mathbb{R}^2$, whose radius is denoted as r_m. The m-th MVNO is located at the cell center.

With wireless network virtualization operation, the whole communication processes are divided into multiple periods, each measured in minutes. Spectrum requirement for a MVNO is highly related to the number of users it will accommodate,

channel condition of those users, QoS those users need. All of these may vary in seconds to minutes due to many reasons, such as user arrivals, movement and departure. At the beginning of each period, MVNOs should predict the required wireless spectrum and acquire spectrum access authorization form the MNO. At the rest of the period, each MVNO provides customized services to the MUs in their respective service cells with newly authorized spectrum. Based on the predicted values, MVNOs acquire wireless spectrum. Denote the bandwidth of wireless spectrum acquired by the m-th MVNO as w_m, for $m \in \mathcal{M}$. We have

$$\sum_{m=1}^{M} w_m \leq W \tag{1}$$

where W denotes the total available bandwidth.

To predict the required wireless spectrum accurately in a period is a hard problem in general. To make it easy to tackle, we assume that all MUs arrive at the service cells with a spatio-temporal Poisson process, the movement of each MU can be modeled as independent Markov process and the sojourn time of each MU before its departure takes on independent exponential distribution. Based on the assumption, the number of active MUs in a service cell obtains a spatial birth-and-death process, whose stationary distribution is a Poisson point process (PPP) [32], [33]. Thus, the number of active MUs in the m-th cell is modeled as a PPP with density λ_m. This is a very common assumption in wireless network modeling and performance analysis [34], [35].

Suppose that transmitted signals are affected by both large-scale path-loss and small-scale flat Rayleigh fading. Thus, the channel between the n-th MU and its associated m-th MVNO is denoted by

$$h_{mn} = \frac{g_{mn}}{\sqrt{1 + L_{mn}^{\alpha}}} \tag{2}$$

where L_{mn} denotes the distance between the m-th MVNO and the n-th MU in the m-th cell, α denotes the path-loss decay factor, and g_{mn} denotes a complex Gaussian random variable with zero mean and unit variance. The instantaneous data rate for the n-th MU in the m-th MVNO is given by

$$R_{mn} = b_{mn} \log_2 \left(1 + \frac{q_{mn} \left| h_{mn} \right|^2}{\Gamma b_{mn} \sigma_0^2} \right) \tag{3}$$

where b_{mn} and q_{mn} denote the bandwidth and power of the n-th MU allocated by the m-th MVNO, respectively, Γ denotes the signal-to-noise ratio (SNR) gap to the information theoretical channel capacity owing to the non-ideal coding and modulation in practice [36], and σ_0^2 denotes the power spectral density of additive white Gaussian noise at all MUs.

III. Dynamic Spectrum Acquisition Optimization Problem Formulation

For the required wireless spectrum prediction, since we have no information on the channels, h_{mn}, we employ the uniform bandwidth allocation and power allocation for the MUs in each cell. Thus, in the m-th cell,

$$b_{mn} = \frac{w_m}{N_m} \text{ and } q_{mn} = \frac{p_m}{N_m} \tag{4}$$

where N_m denotes the number of active MUs in the m-th cell and p_m denotes the total transmission power budget at the m-th MVNO. Since the active MUs in the m-th cell are modeled as a PPP with density λ_m, the average number of MUs in the m-th cell is

$$\mathbb{E}[N_m] = \Lambda_m = \pi r_m^2 \lambda_m. \tag{5}$$

Accordingly, the expected data transmission rate of the n-th MU in the m-th cell is expressed as

$$\mathbb{E}\left[R_{mn}\right] = \sum_{N_m=1}^{\infty} \frac{\Omega}{N_m} \Pr[N_m] \tag{6}$$

where

$$\Omega = \int_0^{\infty} w_m \log_2 \left(1 + \frac{p_m x}{w_m \sigma^2} \right) f_{|h_{ij}|^2}(x)\, dx, \tag{7}$$

$$\Pr[N_m] = \frac{(\Lambda_m)^{N_m}}{N_m!} \exp\left(-\Lambda_m\right). \tag{8}$$

In (7), $\sigma^2 = \Gamma \sigma_0^2$ and $f_{|h_{ij}|^2}(x)$ is the probability density function (PDF) of the random variable $|h_{ij}|^2$. According to [37], we have

$$\sum_{N_m=1}^{\infty} \frac{1}{N_m} \Pr[N_m] = \phi_m \tag{9}$$

where

$$\phi_m = \left(\mathrm{Ei}\left(\Lambda_m\right) - \ln\left(\Lambda_m\right) - C\right) \exp\left(-\Lambda_m\right). \tag{10}$$

In (10), $\mathrm{Ei}(x)$ is the exponential integral function whose series expansion is [37, 5.1.10]

$$\mathrm{Ei}(x) = \sum_{n=1}^{\infty} \frac{x^n}{n \cdot n!} + \ln x + C \tag{11}$$

and C denotes the Euler-Mascheroni constant.

Denote the average data transmission rate threshold for each MU in the m-th cell as $\bar{R}_m$, for $m \in \mathcal{M}$. Note that with limited w_m, to ensure that

$$\mathbb{E}\left[R_{mn}\right] \geq \bar{R}_m, \tag{12}$$

we may increase p_m. Thus, to reasonably allocate wireless spectrum among different MVNOs, we should minimize the sum transmit power at all MVNOs while satisfying the average data transmission rate thresholds, which is formulated as

$$\begin{aligned} \min_{\mathbf{p},\mathbf{w}} \ & \sum_{m=1}^{M} p_m \\ \text{s.t. } & (1),\ (12),\ p_m \geq 0,\ w_m \geq 0,\ \forall\, m \in \mathcal{M} \end{aligned} \tag{13}$$

where $\mathbf{p} = [p_1, p_2, \cdots, p_M]^T$ and $\mathbf{w} = [w_1, w_2, \cdots, w_M]^T$. To proceed, we will first introduce the following proposition.

Proposition 1: The cumulative distribution function (CDF) of $|h_{mn}|^2$ is

$$F_{|h_{mn}|^2}(x) = 1 - \Psi\left(\frac{2}{\alpha}, 1 + \frac{2}{\alpha}, -x r_m^{\alpha}\right) e^{-x} \tag{14}$$

where $\Psi(a, b, z)$ denotes the Kummer's function [37].

Proof: See Appendix A. ■

Using Proposition 1, by taking the first-order derivative with respect to x, $f_{|h_{mn}|^2}(x)$ is

$$f_{|h_{mn}|^2}(x) = \Psi\left(\frac{2}{\alpha}, 1+\frac{2}{\alpha}, -xr_m^\alpha\right)e^{-x} - \frac{d\Psi\left(\frac{2}{\alpha}, 1+\frac{2}{\alpha}, -xr_m^\alpha\right)}{dx}e^{-x}. \quad (15)$$

From [37, 13.4.8], we know

$$\frac{d\Psi(s,t,y)}{dy} = \frac{s}{t}\Psi(s+1, t+1, y). \quad (16)$$

Thus, we have

$$f_{|h_{mn}|^2}(x) = e^{-x}\kappa(x) \quad (17)$$

where

$$\kappa(x) = \Psi\left(\frac{2}{\alpha}, 1+\frac{2}{\alpha}, -xr_m^\alpha\right) + \frac{2r_m^\alpha}{2+\alpha}\Psi\left(1+\frac{2}{\alpha}, 2+\frac{2}{\alpha}, -xr_m^\alpha\right). \quad (18)$$

Substituting (17) into (12), we obtain

$$\xi \geq \bar{R}_m \quad (19)$$

where

$$\xi = \phi_m \int_0^\infty w_m \log_2\left(1+\frac{p_m x}{w_m\sigma^2}\right)e^{-x}\kappa(x)\,dx. \quad (20)$$

It is noted that on the left-hand side of (19), the integral result ξ is difficult to obtain. Furthermore, when the integrand has a non-negligible tail, even the numerical integration is complicated and time-consuming. In this paper, we propose to apply the half-range Gauss-Hermite quadrature (HR-GHQ) to approximate the integral on the left-hand side of (19) with high accuracy [38], [39].

Based on [39], a K-point HR-GHQ can be written as

$$\int_0^\infty e^{-t^2}\zeta(t)\,dt \approx \sum_{k=1}^K a_k\zeta(t_k) \quad (21)$$

where both the weights $\{a_k\}_{k=1}^K$ and abscissas $\{t_k\}_{k=1}^K$ are real numbers. By letting $x = t^2$, we have

$$\xi = \phi_m \int_0^\infty 2w_m t\log_2\left(1+\frac{p_m t^2}{w_m\sigma^2}\right)e^{-t^2}\kappa\left(t^2\right)dt. \quad (22)$$

Applying the K-point HR-GHQ, we obtain

$$\xi \approx \sum_{k=1}^K w_m\eta_{mk}\log_2\left(1+\frac{p_m t_{mk}^2}{w_m\sigma^2}\right) \quad (23)$$

where $\eta_{mk} = 2\phi_m a_{mk}t_{mk}\kappa\left(t_{mk}^2\right)$, and both the weights $\{a_{mk}\}$ and abscissas $\{t_{mk}\}$ are real numbers.

Substituting (23) into problem (13), we have the following optimization problem

$$\begin{aligned}\min_{\mathbf{p},\mathbf{w}} \ & \sum_{m=1}^M p_m \\ \text{s.t.} \ & \sum_{k=1}^K w_m\eta_{mk}\log_2\left(1+\frac{p_m t_{mk}^2}{w_m\sigma^2}\right) \geq \bar{R}_m, \\ & (1),\ p_m \geq 0,\ w_m \geq 0,\ \forall\, m \in \mathcal{M}. \end{aligned} \quad (24)$$

Problem (24) is convex in terms of optimization variables $\mathbf{p}$ and $\mathbf{w}$. It can be solved efficiently using the interior point method [40]. However, to solve problem (24) in a centralized manner requires a central node. If the central node is under cyberattack, all the M MVNOs are vulnerable. In addition, since the M MVNOs may belong to different network providers, the information exchanging among different nodes should be as less as possible. Furthermore, the management overhead increases with the increase of M which causes that the wireless downlink communication system is not scalable. To deal with the aforementioned problems, we propose a blockchain-based distributed ADMM algorithm [41], [42] for dynamic spectrum acquisition in this paper.

IV. Blockchain-Based Distributed ADMM Algorithm for Dynamic Spectrum Acquisition

By introducing auxiliary variable $\mathbf{z} = [z_1, z_2, \cdots, z_M]^T$, problem (24) is reformulated as

$$\begin{aligned}\min_{\mathbf{p},\mathbf{w},\mathbf{z}} \ & \sum_{m=1}^M p_m && \text{(25a)}\\ \text{s.t.} \ & \sum_{k=1}^K w_m\eta_{mk}\log_2\left(1+\frac{p_m t_{mk}^2}{w_m\sigma^2}\right) \geq \bar{R}_m, && \text{(25b)}\\ & \sum_{m=1}^M w_m \leq W, && \text{(25c)}\\ & \mathbf{w}-\mathbf{z} = \mathbf{0}, && \text{(25d)}\\ & p_m \geq 0,\ w_m \geq 0,\ z_m \geq 0,\ \forall\, m \in \mathcal{M}. && \text{(25e)}\end{aligned}$$

Denote the feasible region of constraint (25c) and $z_m \geq 0$, $\forall\, m \in \mathcal{M}$ as $\mathcal{Z}$, its indicator function is defined as

$$\mathbb{I}_{\mathcal{Z}}(\mathbf{z}) = \begin{cases} 0, & \text{if } \mathbf{z} \in \mathcal{Z}, \\ \infty, & \text{otherwise.} \end{cases} \quad (26)$$

Similarly, denote the feasible region of constraint (25b), $p_m \geq 0$ and $w_m \geq 0$, $\forall\, m \in \mathcal{M}$ as $\mathcal{C}$, its indicator function can be defined as

$$\mathbb{I}_{\mathcal{C}}(\mathbf{p},\mathbf{w}) = \begin{cases} 0, & \text{if } (\mathbf{p},\mathbf{w}) \in \mathcal{C}, \\ \infty, & \text{otherwise.} \end{cases} \quad (27)$$

With (26) and (27), problem (25) can be rewritten in ADMM form as follows

$$\begin{aligned}\min_{\mathbf{p},\mathbf{w},\mathbf{z}} \ & \sum_{m=1}^M p_m + \mathbb{I}_{\mathcal{Z}}(\mathbf{z}) + \mathbb{I}_{\mathcal{C}}(\mathbf{p},\mathbf{w}) && \text{(28a)}\\ \text{s.t.} \ & \mathbf{w}-\mathbf{z} = \mathbf{0}. && \text{(28b)}\end{aligned}$$

Thus, the augmented Lagrangian (using the scaled dual variable) of problem (28) is given by

$$\mathcal{L}_\nu(\mathbf{p},\mathbf{w},\mathbf{z},\mathbf{u}) = \sum_{m=1}^M p_m + \mathbb{I}_{\mathcal{Z}}(\mathbf{z}) + \mathbb{I}_{\mathcal{C}}(\mathbf{p},\mathbf{w}) + \frac{\nu}{2}\|\mathbf{w}-\mathbf{z}+\mathbf{u}\|_2^2 \quad (29)$$

where $\mathbf{u} = [u_1, u_2, \cdots, u_N]^T$ is the dual variable for the constraint (28b) and $\nu > 0$ is the penalty parameter. From problem (28), it is observed that the variables can be split into

two groups: $\{\mathbf{p}, \mathbf{w}\}$ and $\mathbf{z}$. Furthermore, the objective function can be separable accordingly. Therefore, the ADMM algorithm can be applied to solve problem (28) by iteratively updating $\mathbf{p}, \mathbf{w}$, $\mathbf{z}$ and $\mathbf{u}$.

In the $(l+1)$-th iteration, given $\{\mathbf{p}^{(l)}, \mathbf{w}^{(l)}, \mathbf{z}^{(l)}, \mathbf{u}^{(l)}\}$ which is optimal in the l-th iteration, the optimization variables are updated sequentially as follows.

Step 1: Given $\{\mathbf{z}^{(l)}, \mathbf{u}^{(l)}\}$, we solve the following optimization problem

$$\{\mathbf{p}^{(l+1)}, \mathbf{w}^{(l+1)}\} = \arg\max_{\mathbf{p},\mathbf{w}} \mathcal{L}_\nu \left(\mathbf{p}, \mathbf{w}, \mathbf{z}^{(l)}, \mathbf{u}^{(l)}\right). \quad (30)$$

Problem (30) is equivalent to

$$\begin{aligned} \min_{\mathbf{p},\mathbf{w}} \ & \sum_{m=1}^{M} p_m + \frac{\nu}{2} \sum_{m=1}^{M} \left(w_m - z_m^{(l)} + u_m^{(l)}\right)^2 \\ \text{s.t. } & \text{(25b)}, \ w_m \geq 0, \ p_m \geq 0, \ \forall\, m \in \mathcal{M}. \end{aligned} \quad (31)$$

It is noted that problem (31) can be decomposed into M subproblems. Each subproblem solves

$$\begin{aligned} \min_{p_m, w_m} \ & p_m + \frac{\nu}{2} \left(w_m - z_m^{(l)} + u_m^{(l)}\right)^2 \\ \text{s.t. } & \sum_{k=1}^{K} w_m \eta_{mk} \log_2 \left(1 + \frac{p_m t_{mk}^2}{w_m \sigma^2}\right) \geq \bar{R}_m, \\ & w_m \geq 0, p_m \geq 0. \end{aligned} \quad (32)$$

Problem (32) is a convex problem and can be solved efficiently using interior point method [40].

Step 2: Given $\{\mathbf{p}^{(l+1)}, \mathbf{w}^{(l+1)}, \mathbf{u}^{(l)}\}$, we solve the following optimization problem

$$\mathbf{z}^{(l+1)} = \arg\max_{\mathbf{z}} \mathcal{L}_\nu \left(\mathbf{p}^{(l+1)}, \mathbf{w}^{(l+1)}, \mathbf{z}, \mathbf{u}^{(l)}\right). \quad (33)$$

Problem (33) is equivalent to

$$\min_{\mathbf{z}} \ \left\|\mathbf{w}^{(l+1)} - \mathbf{z} + \mathbf{u}^{(l)}\right\|_2^2 \quad (34)$$

$$\text{s.t. } \|\mathbf{z}\|_1 \leq W, \ z_m \geq 0, \ \forall\, m \in \mathcal{M}. \quad (35)$$

Problem (34) is a convex ℓ_1 ball projection problem [43]. Its closed-form solution is obtained as follows.

If $\|\mathbf{w}^{(l+1)} + \mathbf{u}^{(l)}\|_1 > W$, we have

$$z_m^{(l+1)} = \max\left\{w_m^{(l+1)} + u_m^{(l)} - \beta, 0\right\} \quad (36)$$

where

$$\beta = \frac{1}{\tau}\left(\sum_{m=1}^{\tau} \varphi_m - W\right), \quad (37)$$

$$\tau = \max_{1 \leq i \leq M} \left\{ i \left| \varphi_i - \frac{1}{i}\left(\sum_{m=1}^{i} \varphi_m - W\right) > 0 \right.\right\}, \quad (38)$$

and $\boldsymbol{\varphi} = [\varphi_1, \varphi_2, \cdots, \varphi_M]^T$ denotes the vector obtained by sorting $\mathbf{w}^{(l+1)} + \mathbf{u}^{(l)}$ in a descending order.

If $\|\mathbf{w}^{(l+1)} + \mathbf{u}^{(l)}\|_1 \leq W$, we have

$$z_m^{(l+1)} = w_m^{(l+1)} + u_m^{(l)}. \quad (39)$$

Step 3: Given $\{\mathbf{w}^{(l+1)}, \mathbf{z}^{(l+1)}\}$, we solve the following optimization problem

$$\mathbf{u}^{(l+1)} = \arg\max_{\mathbf{u}} \mathcal{L}_\nu \left(\mathbf{p}^{(l+1)}, \mathbf{w}^{(l+1)}, \mathbf{z}^{(l+1)}, \mathbf{u}\right). \quad (40)$$

The closed-form solution to problem (40) is

$$\mathbf{u}^{(l+1)} = \mathbf{w}^{(l+1)} - \mathbf{z}^{(l+1)} + \mathbf{u}^{(l)}. \quad (41)$$

Thus, the whole blockchain-based distributed ADMM algorithm for dynamic spectrum acquisition is summarized in Algorithm 1.

Algorithm 1 Blockchain-Based Distributed ADMM Algorithm for Dynamic Spectrum Acquisition

1: **Initialize**: $z_m^{(0)} = 0$ and $u_m^{(0)} = 0 \ \forall\, m \in \mathcal{M}$; $\nu = 0$; $l = 0$;
2: **Repeat**:
  Local Computation:
    Get $z_m^{(l)}$ and $u_m^{(l)}$ from blockchain;
    Obtain $p_m^{(l+1)}$ and $w_m^{(l+1)}$ by solving (32);
    Send $w_m^{(l+1)}$ to ADMM aggregator on blockchain;
  Blockchain Computation:
    S_1: Obtain $\mathbf{z}^{(l+1)}$ and $\mathbf{u}^{(l+1)}$;
  $l = l + 1$;
  Until Convergence.
3: S_2: All MVNOs pay for their spectrum and get authorization from the MNO according to convergent result computed by S_1.

In Algorithm 1, both S_1 and S_2 are smart contract deployed on the blockchain. Smart contract S_1 receives the local computational result $w_m^{(l+1)}$ sent from every MVNO as input, and compute $\mathbf{z}^{(l+1)}$ and $\mathbf{u}^{(l+1)}$. Based on the assumption that most MVNOs are reliable, the final correctness of $\mathbf{z}^{(l+1)}$ and $\mathbf{u}^{(l+1)}$ can be ensured even if there are some malicious participants due to the consensus mechanism. If the convergent condition is satisfied, the result will be sent to smart contract S_2. If not, result will be sent to MVNOs. Smart contract S_2 receives convergent result sent from S_1 as input. Then it bills all the MVNOs and authorizes them to use their acquired spectrum according to the final convergent result.

Smart contract S_1 and S_2 act like MNO in traditional centralized solutions. $\mathbf{w}^{(l+1)}$ can be viewed as the spectrum MVNOs demand, $\mathbf{z}^{(l+1)}$ means the spectrum MNO can provide to MVNOs taking all network demands into consideration. Iteration is similar to the negotiation process between MNO and MVNOs. After several round negotiations, a final agreement between MNO and MVNOs will be achieved.

Remark 1: Blockchains provide a method for providing a transparent, trustless platform for data computation. This makes a blockchain the perfect platform for conducting the aggregation step of ADMM, allowing all participants to audit the progress of the algorithm, the accuracy of the solution, and the veracity of their scheduled commitments. Further, ADMM is a natural fit for implementation on a blockchain, as it guarantees convergence yet has a computationally cheap aggregation step (minimizing the burden of verification) [19].

V. Optimal Power and Spectrum Allocation with Known System Parameters

In this paper, we propose a dynamic spectrum acquisition scheme. To fairly compare the performance of our proposed scheme with the fixed spectrum allocation scheme and other schemes, with known system parameters, we propose to investigate the actually required minimum sum transmit power of M MVNOs subject to that the data transmission rate thresholds for all MUs in M cells are satisfied. With our proposed dynamic spectrum acquisition scheme and other spectrum allocation schemes, the bandwidth of wireless spectrum of the m-th MVNO, i.e., w_m, is known. Thus, the aforementioned optimization problem is decoupled into M transmit power minimization subproblems. For the transmit power minimization subproblem of the m-th MVNO, with known system parameters, we should study the power and spectrum allocation optimization problem among all MUs in the m-th cell subject to that the data transmission rate thresholds for all MUs in the m-th cell are satisfied.

In the m-th cell, when the actual number of MUs, N_m, and the channel between the n-th MU and its associated m-th MVNO, h_{mn}, are known for $n \in \mathcal{N}_m = \{1, 2, \cdots, N_m\}$, the power and spectrum allocation optimization problem is formulated as

$$\min_{\mathbf{q}_m, \mathbf{b}_m} \quad \sum_{n=1}^{N_m} q_{mn} \tag{42a}$$

$$\text{s.t.} \quad \sum_{n=1}^{N_m} b_{mn} \leq w_m, \tag{42b}$$

$$b_{mn} \log_2 \left(1 + \frac{q_{mn} |h_{mn}|^2}{b_{mn}\sigma^2}\right) \geq \tilde{R}_m, \tag{42c}$$

$$q_{mn} \geq 0, \ b_{mn} \geq 0, \ \forall \ n \in \mathcal{N}_m \tag{42d}$$

where $\tilde{R}_m$ denotes the data transmission rate threshold for each MU in the m-th cell, $\mathbf{q}_m = [q_{m1}, q_{m2}, \cdots, q_{mN_m}]^T$, and $\mathbf{b}_m = [b_{m1}, b_{m2}, \cdots, b_{mN_m}]^T$. To continue, we need the following proposition.

Proposition 2: For problem (42), the optimal $\mathbf{q}_m$ and $\mathbf{b}_m$ should satisfy that constraint (42c) are all active, i.e.,

$$b_{mn} \log_2 \left(1 + \frac{q_{mn} |h_{mn}|^2}{b_{mn}\sigma^2}\right) = \tilde{R}_m, \ \forall \ n \in \mathcal{N}_m \tag{43}$$

Proof: See Appendix B. ■

From Proposition 2, problem (42) is equivalently written as

$$\min_{\mathbf{b}_m} \quad \sum_{n=1}^{N_m} \frac{b_{mn}\sigma^2}{|h_{mn}|^2} \left(2^{\frac{\tilde{R}_m}{b_{mn}}} - 1\right)$$

$$\text{s.t.} \quad \sum_{n=1}^{N_m} b_{mn} \leq w_m, \ b_{mn} \geq 0, \ \forall n \in \mathcal{N}_m. \tag{44}$$

Problem (44) is convex. In the following proposition, we propose to solve problem using the bisection search.

Proposition 3: The closed-form optimal solution to problem (44), denoted by b_{mn}^o, is

$$b_{mn}^o = \frac{\tilde{R}_m \ln 2}{1 + \mathcal{W}\left(\frac{\mu^o |h_{mn}|^2 - \sigma^2}{e\sigma^2}\right)}, \ \forall \ n \in \mathcal{N}_m \tag{45}$$

where $\mathcal{W}(x)$ denotes the Lambert $\mathcal{W}$ function of x [44] and $\mu^o > 0$ is a constant which satisfies $\sum_{n=1}^{N_m} b_{mn} = w_m$. The value of μ^o can be found by the bisection search over $[\mu_{\min}, \mu_{\max}]$ with

$$\mu_{\min} = \frac{\chi}{\max_n |h_{mn}|^2} \text{ and } \mu_{\max} = \frac{\chi}{\min_n |h_{mn}|^2} \tag{46}$$

where

$$\chi = \sigma^2 \left(\frac{N_m \tilde{R}_m \ln 2}{w_m} - 1\right) \exp\left(\frac{N_m \tilde{R}_m \ln 2}{w_m}\right) + \sigma^2. \tag{47}$$

Proof: See Appendix C. ■

VI. Simulation Results

In this section, we evaluate the performance of our proposed dynamic spectrum acquisition through simulations. We consider a wireless downlink communication system with $M = 6$ MVNOs. Each MVNO serves the MUs in a cell. Since each MVNO uses different wireless spectrum for transmission, there is no co-channel interference. Thus, the overlap of different cells will not cause a problem. We assume that the radii and the corresponding user densities of the $M = 6$ cells are ($r_1 = 80$ m, $\lambda_1 = 1200$ persons/km^2), ($r_2 = 80$ m, $\lambda_2 = 800$ persons/km^2), ($r_3 = 100$ m, $\lambda_3 = 800$ persons/km^2), ($r_4 = 100$ m, $\lambda_4 = 1000$ persons/km^2), ($r_5 = 120$ m, $\lambda_5 = 1000$ persons/km^2), and ($r_6 = 120$ m, $\lambda_6 = 1200$ persons/km^2). The total available bandwidth is 100 MHz. The path-loss decay factor is 3.76 [45]. We assume that $\sigma^2 = \Gamma\sigma_0^2 = -150.9$ dBm/Hz [45]. In (21), a $K = 500$-point HR-GHQ is employed. If not specified, the average data transmission rate threshold in (12) and the data transmission rate threshold in (42) are $\bar{R}_1 = \tilde{R}_1 = 2$ Mbps, $\bar{R}_2 = \tilde{R}_2 = 0.5$ Mbps, $\bar{R}_3 = \tilde{R}_3 = 0.5$ Mbps, $\bar{R}_4 = \tilde{R}_4 = 1$ Mbps, $\bar{R}_5 = \tilde{R}_5 = 1$ Mbps, and $\bar{R}_6 = \tilde{R}_6 = 2$ Mbps.

In Fig. 1, we show the convergence performance of Algorithm 1. From Fig. 1, it is observed that our proposed Algorithm 1 converges for about 10 iterations. Furthermore, the parameters and final convergent results are summarized in Table I. For a MVNO, it is found that the more bandwidth is needed when more throughput is expected to provide in most cases. Throughput expected to provide for a MVNO can be computed by multiplying the average number of MUs in the cell with the average data transmission rate threshold, i.e. $\mathbb{E}[N_m]\bar{R}_m$. But it is also spotted that although the throughput expected to provide of the 1^{st} MVNO is more than that of the 5^{th} MVNO, the acquired spectrum is less. The reason is that the service cell radius of the 5^{th} MVNO is much larger than that of the 1^{st} MVNO. In large service cells, more power will be used to compensate the distance-related large-scale path-loss to satisfy the QoS constraints for cell-edge MUs. In order to minimize the total power used in all MVNO, more spectrum should be allocated to the large cell.

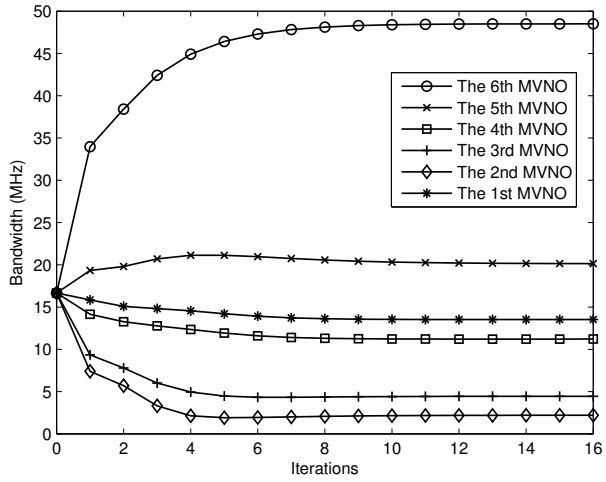

Fig. 1. Bandwidth versus iterations; the convergence performance of Algorithm 1.

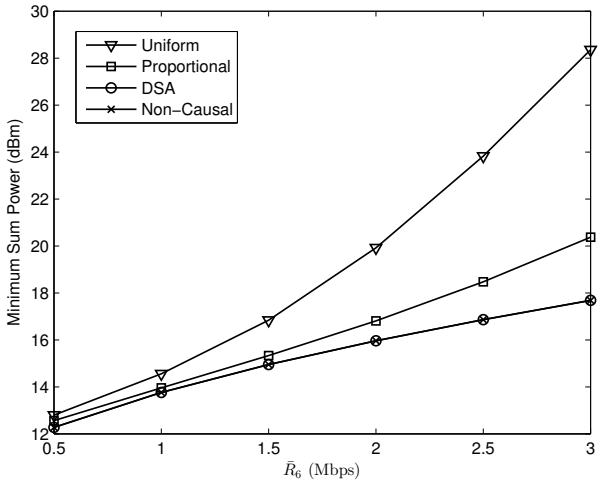

Fig. 2. Minimum sum power versus $\bar{R}_6$; comparison of our proposed dynamic spectrum acquisition scheme, the "Uniform" scheme, the "Proportional" scheme, and the "Non-Causal" scheme.

TABLE I
SUMMARY OF PARAMETERS AND RESULTS IN FIG. 1

MVNO	r_m (m)	λ_m (/km^2)	$\mathbb{E}[N_m]$	$\bar{R}_m$ (Mbps)	$\mathbb{E}[N_m]\bar{R}_m$ (Mbps)	w_m (MHz)
1	80	1200	24	2	48	13.51
2	80	800	16	0.5	8	2.2
3	100	800	25	0.5	12.5	4.44
4	100	1000	31	1	31	11.21
5	120	1000	45	1	45	20.14
6	120	1200	54	2	108	48.5

In Fig. 2, we present the minimum sum power comparison of different schemes for different values of the average data transmission rate threshold in the 6-th cell, $\bar{R}_6$. In the legend, "DSA" denotes our proposed dynamic spectrum acquisition scheme. "Uniform" denotes that the total available bandwidth is uniformly allocated to $M = 6$ MVNOs. "Proportional" denotes that the total available bandwidth is allocated to MVNOs proportionally according to $\mathbb{E}[N_m]\bar{R}_m$. "Non-Causal" denotes that assuming the number of active MUs in all cells and all the channels, h_{mn}, $\forall\ n \in \mathcal{N}_m,\ m \in \mathcal{M}$, are known non-causally, we solve the joint sum transmit power minimization and bandwidth allocation optimization problem subject to that the data transmission rate thresholds for all MUs in M cells are satisfied. From Fig. 2, it is observed that our proposed dynamic spectrum acquisition scheme achieves almost the same minimum sum power as the "Non-Causal" scheme.

In Fig. 3, we present the bandwidth allocation comparison of different schemes with the parameters in Table I. From Fig. 3, it is found that the allocated bandwidth of our proposed dynamic spectrum acquisition scheme is almost the same as that of the "Non-Causal" scheme.

In Fig. 4, we vary the value of λ_6 while remaining other parameters unchanged in Table 1 and present the minimum sum power comparison of different schemes. In Fig. 5, we present the corresponding bandwidth allocation of our proposed dynamic spectrum acquisition scheme for all MVNOs. From Fig. 4, it is shown that almost the same minimum sum power is obtained by our proposed dynamic spectrum acquisition scheme and the "Non-Causal" scheme.

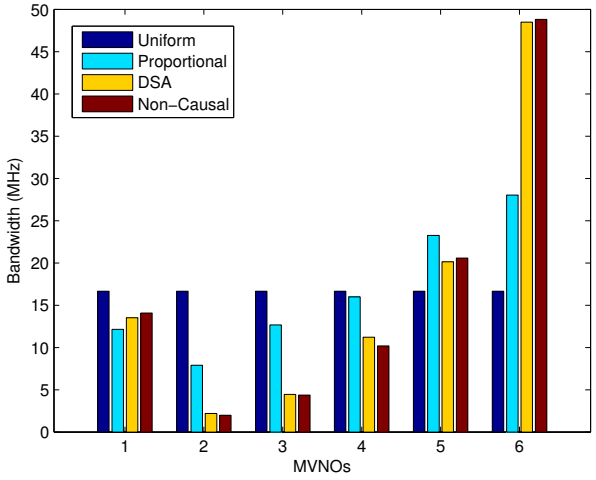

Fig. 3. Bandwidth allocation comparison of our proposed dynamic spectrum acquisition scheme, the "Uniform" scheme, the "Proportional" scheme, and the "Non-Causal" scheme when $\bar{R}_6 = 2$ Mbps.

VII. CONCLUSION

In this paper, we have proposed a decentralized blockchain based dynamic spectrum acquisition scheme for a wireless downlink communication system with multiple MVNOs. It is shown through simulation results that our proposed dynamic spectrum acquisition scheme achieves almost the same minimum sum power as the non-causal scheme which assumes the number of active MUs in all cells and all the channels are known non-causally for optimal dynamic spectrum allocation. And our proposed dynamic spectrum acquisition scheme outperforms uniform allocating and proportional allocating schemes. By using the blockchain system to implement the dynamic spectrum acquisition scheme, many advantages can

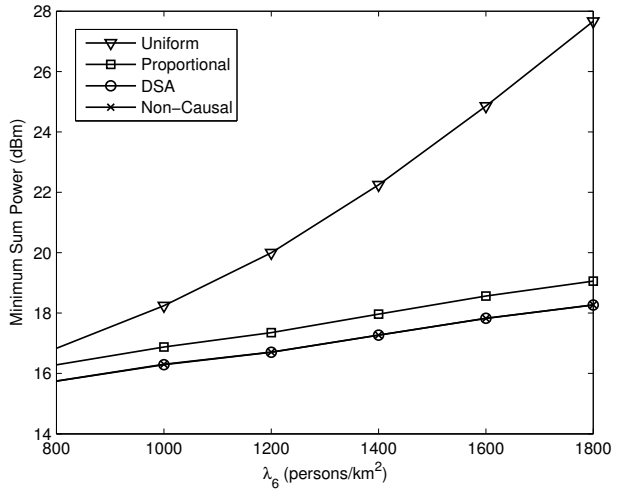

Fig. 4. Minimum sum power versus λ_6; comparison of our proposed dynamic spectrum acquisition scheme, the "Uniform" scheme, the "Proportional" scheme, and the "Non-Causal" scheme when $\bar{R}_1 = \tilde{R}_1 = 2$ Mbps, $\bar{R}_2 = \tilde{R}_2 = 0.5$ Mbps, $\bar{R}_3 = \tilde{R}_3 = 0.5$ Mbps, $\bar{R}_4 = \tilde{R}_4 = 1$ Mbps, $\bar{R}_5 = \tilde{R}_5 = 1$ Mbps, and $\bar{R}_6 = \tilde{R}_6 = 2$ Mbps.

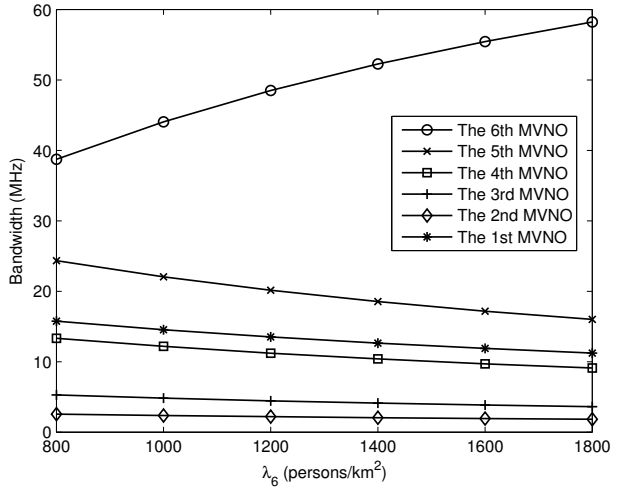

Fig. 5. Bandwidth allocation of all MVNOs versus λ_6; our proposed dynamic spectrum acquisition scheme when $\bar{R}_1 = \tilde{R}_1 = 2$ Mbps, $\bar{R}_2 = \tilde{R}_2 = 0.5$ Mbps, $\bar{R}_3 = \tilde{R}_3 = 0.5$ Mbps, $\bar{R}_4 = \tilde{R}_4 = 1$ Mbps, $\bar{R}_5 = \tilde{R}_5 = 1$ Mbps, and $\bar{R}_6 = \tilde{R}_6 = 2$ Mbps.

be obtained at the expense of extra computation and storage cost in each MVNO. Advantages can be listed as:

- By delegating all the computational and data operating work to the MVNOs and the blockchain, a lot of management cost of the MNO can be avoided.
- Spectrum acquisition, billing and authorization can be performed automatically with the help of smart contracts deployed on the blockchain. The processing delay is decreased sharply which makes real-time dynamic spectrum access possible.
- Due to the transparency of the blockchain, the MVNOs can be ensured that they are charged fairly.
- During the spectrum acquisition process, MUs related data doesn't need to exchange in the network. Thus, MUs' privacy can be protected.
- The blockchain system is more robust to cyberattack. The network is safe and reliable until most of the participant MVNOs have been controlled by the attacker.

Appendix A
Proof of Proposition 1

According to the definition of the CDF, we have

$$F_{|h_{mn}|^2}(x) = \Pr\left(|g_{mn}|^2 \le x\left(1 + L_{mn}^{\alpha}\right)\right). \quad (48)$$

Since g_{mn} is a complex Gaussian random variable with zero mean and unit variance, $|g_{ij}|^2$ is an exponentially distributed random variable. Furthermore, the location of the n-th MU in the m-th cell is uniformly distributed in $\mathcal{D}_m$ with the PDF of $1/(\pi r_m^2)$. By using polar coordinates, we obtain

$$F_{|h_{mn}|^2}(x) = \int_0^{r_m}\int_{-\pi}^{\pi} \frac{1}{\pi r_m^2}\left(1 - e^{-x(1+y^{\alpha})}\right) y d\theta dy. \quad (49)$$

After some mathematical manipulation, we obtain

$$F_{|h_{mn}|^2}(x) = 1 - \frac{2}{r_m^2}e^{-x}\int_0^{r_m} y e^{-xy^{\alpha}} dy. \quad (50)$$

Let $t = xy^{\alpha}$. $F_{|h_{mn}|^2}(x)$ is reexpressed as

$$\begin{aligned} F_{|h_{mn}|^2}(x) &= 1 - \frac{2}{r_m^2}e^{-x}\int_0^{xr_m^{\alpha}} t^{\frac{1}{\alpha}} x^{-\frac{1}{\alpha}} e^{-t} d\left(t^{\frac{1}{\alpha}} x^{-\frac{1}{\alpha}}\right) \\ &= 1 - \frac{2}{\alpha r_m^2} x^{-\frac{2}{\alpha}} e^{-x}\int_0^{xr_m^{\alpha}} t^{\frac{2}{\alpha}-1} e^{-t} dt \\ &= 1 - \frac{2}{\alpha}\left(xr_m^{\alpha}\right)^{-\frac{2}{\alpha}} \gamma\left(\frac{2}{\alpha}, xr_m^{\alpha}\right) e^{-x} \end{aligned} \quad (51)$$

where $\gamma(s,x) = \int_0^x t^{s-1}e^{-t}dt$ denotes the lower incomplete gamma function. Because $\Psi(s, 1+s, -x) = sx^{-s}\gamma(s,x)$ [37, 6.5.12], we obtain (14).

Appendix B
Proof of Proposition 2

We prove Proposition 2 by contradiction. Assume that $\mathbf{q}_m^{\star} = [q_{m1}^{\star}, q_{m2}^{\star}, \cdots, q_{mN_m}^{\star}]^T$ is the optimal solution to problem (42) such that there exists $n \in \mathcal{N}_m$ which satisfy

$$b_{mn}\log_2\left(1 + \frac{q_{mn}|h_{mn}|^2}{b_{mn}\sigma^2}\right) > \tilde{R}_m. \quad (52)$$

We can choose a proper real scalar $\Delta > 0$ such that

$$b_{mn}\log_2\left(1 + \frac{(q_{mn}^{\star} - \Delta)|h_{mn}|^2}{b_{mn}\sigma^2}\right) = \tilde{R}_m. \quad (53)$$

Note that $[q_{m1}^{\star}, \cdots, q_{m(n-1)}^{\star}, q_{mn}^{\star} - \Delta, q_{m(n+1)}^{\star}, \cdots, q_{mN_m}^{\star}]^T$ is also feasible and has smaller objective value than $\mathbf{q}_m^{\star}$. This contradicts that $\mathbf{q}_m^{\star}$ is the optimal solution.

APPENDIX C
PROOF OF PROPOSITION 3

The Lagrangian of problem (44) is given by

$$\tilde{\mathcal{L}} = \sum_{n=1}^{N_m} \frac{b_{mn}\sigma^2}{|h_{mn}|^2}\left(e^{\frac{\tilde{R}_m \ln 2}{b_{mn}}} - 1\right) + \mu\left(\sum_{n=1}^{N_m} b_{mn} - w_m\right) \quad (54)$$

where $\mu \geq 0$ denotes the Lagrange multiplier associated with the constraint $\sum_{n=1}^{N_m} b_{mn} \leq w_m$. Since problem (44) is convex, the Karush-Kuhn-Tucker (KKT) conditions are both necessary and sufficient for the global optimality of problem (44). It can be verified that $\sum_{n=1}^{N_m} b_{mn} = w_m$ must hold for problem (42). From KKT conditions, we have $\mu^o > 0$ where μ^o denotes the optimal dual solution to problem (44).

Taking the first-order partial derivative of $\tilde{\mathcal{L}}$ with respect to b_{mn}, we have

$$\frac{\partial \tilde{\mathcal{L}}}{\partial b_{mn}} = \frac{\sigma^2}{|h_{mn}|^2}\left(\left(1 - \frac{\tilde{R}_m \ln 2}{b_{mn}}\right)e^{\frac{\tilde{R}_m \ln 2}{b_{mn}}} - 1\right) + \mu \quad (55)$$

From KKT conditions, we have

$$\left(\frac{\tilde{R}_m \ln 2}{b^o_{mn}} - 1\right)e^{\frac{\tilde{R}_m \ln 2}{b^o_{mn}} - 1} = \frac{\mu^o |h_{mn}|^2 - \sigma^2}{e\sigma^2}. \quad (56)$$

According to the definition of Lambert $\mathcal{W}$ function, we obtain the optimal b^o_{mn} as in (45). In (45), there exists an unknown parameter μ^o. The value of μ^o should satisfy $\sum_{n=1}^{N_m} b_{mn} = w_m$.

In (45), since

$$\frac{\mu^o |h_{mn}|^2 - \sigma^2}{e\sigma^2} \geq -1, \quad (57)$$

$\mathcal{W}(x)$ is a monotonically increasing function. Accordingly, b^o_{mn} is a monotonically decreasing function of $|h_{mn}|^2$. Thus, we have

$$\begin{aligned} &\frac{\tilde{R}_m \ln 2}{1 + \mathcal{W}\left(\frac{\mu^o \max_n |h_{mn}|^2 - \sigma^2}{e\sigma^2}\right)} \leq b^o_{mn} \\ &\leq \frac{\tilde{R}_m \ln 2}{1 + \mathcal{W}\left(\frac{\mu^o \min_n |h_{mn}|^2 - \sigma^2}{e\sigma^2}\right)} \end{aligned} \quad (58)$$

Summing each term in (58) from $n = 1$ to $n = N_m$, we obtain

$$\begin{aligned} &\frac{N_m \tilde{R}_m \ln 2}{1 + \mathcal{W}\left(\frac{\mu^o \max_n |h_{mn}|^2 - \sigma^2}{e\sigma^2}\right)} \leq w_m \\ &\leq \frac{N_m \tilde{R}_m \ln 2}{1 + \mathcal{W}\left(\frac{\mu^o \min_n |h_{mn}|^2 - \sigma^2}{e\sigma^2}\right)} \end{aligned} \quad (59)$$

According to the definition of Lambert $\mathcal{W}$ function, we have

$$\mu_{\min} \leq \mu^o \leq \mu_{\max} \quad (60)$$

where $\mu_{\min}$ and $\mu_{\max}$ are defined in (46).

REFERENCES

[1] N. Panwar, S. Sharma, and A. K. Singh, "A survey on 5G: The next generation of mobile communication," *Phys. Commun.*, vol. 18, pp. 64-84, Mar. 2016.

[2] Z. Ding, Z. Yang, P. Fan, and H. V. Poor, "On the performance of nonorthogonal multiple access in 5G systems with randomly deployed users," *IEEE Signal Process. Lett.*, vol. 21, no. 12, pp. 1501-1505, Dec. 2014.

[3] Y. Li, M. Jiang, Q. Zhang, Q. Li, and J. Qin, "Secure beamforming in downlink MISO nonorthogonal multiple access systems," *IEEE Trans. Veh. Technol.*, vol. 66, no. 8, pp. 7563-7567, Aug. 2017.

[4] Y. Li, M. Jiang, Q. Zhang, Q. Li, and J. Qin, "Cooperative non-orthogonal multiple access in multiple-input-multiple-output channels," *IEEE Trans. Wireless Commun.*, vol. 17, no. 3, pp. 2068-2079, Mar. 2018.

[5] A. Y. Ding and M. Janssen, "Opportunities for applications using 5G networks: Requirements, challenges, and outlook," in *Proc. of International Conference on Telecommunications and Remote Sensing, 2018*, pp. 27-34.

[6] C. Liang and F. R. Yu, "Wireless network virtualization: A survey, some research issues and challenges," *IEEE Comm. Surveys Tuts.*, vol. 17, no. 1, pp. 358-380, First Quart. 2015.

[7] L. Zhao, M. Li, Y. Zaki, A. Timm-Giel, and C. Görg, "LTE virtualization: From theoretical gain to practical solution," in *Proc. International Teletraffic Congress, 2011*, pp. 71-78.

[8] 3GPP TR 22.852, "Study on radio access network (RAN) sharing enhancements," Jun. 2013.

[9] R. Kokku, R. Mahindra, H. Zhang, and S. Rangarajan, "NVS: A substrate for virtualizing wireless resources in cellular networks," *IEEE/ACM Trans. Netw.*, vol. 20, no. 5, pp. 1333-1346, Oct. 2012.

[10] X. Costa-Perez, J. Swetina, T. Guo, R. Mahindra, and S. Rangarajan, "Radio access network virtualization for future mobile carrier networks," *IEEE Commun. Mag.*, vol. 51, no. 7, pp. 27-35, Jul. 2013.

[11] M. I. Kamel, L. B. Le, and A. Girard, "LTE wireless network virtualization: Dynamic slicing via flexible scheduling," in *Proc. IEEE VTC, 2014*, pp. 1-5.

[12] M. Kalil, A. Moubayed, A. Shami, and A. Al-Dweik, "Efficient low-complexity scheduler for wireless resource virtualization," *IEEE Wireless Commun. Lett.*, vol. 5, no. 1, pp. 56-59, Feb. 2016.

[13] Y. Zhang, S. Bi, and Y. J. A. Zhang, "Joint spectrum reservation and on-demand request for mobile virtual network operators," *IEEE Trans. Commun.*, vol. 66, no. 7, pp. 2966-2977, Jul. 2018.

[14] S. Nakamoto, "Bitcoin: A peer-to-peer electronic cash system," 2008. [Online]. Available: https://bitcoin.org/bitcoin.pdf

[15] K. Gai, K.-K. R. Choo, and L. Zhu, "Blockchain-enabled reengineering of cloud datacenters," *IEEE Cloud Comput.*, vol. 5, no. 6, pp. 21-25, Nov. 2018.

[16] P. K. Sharma, S. Singh, Y. S. Jeong, and J. H. Park, "DistBlockNet: A distributed blockchains-based secure SDN architecture for IoT networks," *IEEE Commun. Mag.*, vol. 55, no. 9, pp. 78-85, Sept. 2017.

[17] Z. Xiong, S. Feng, W. Wang, D. Niyato, P. Wang, and Z. Han, "Cloud/fog computing resource management and pricing for blockchain networks," *IEEE Internet Things J.*, to be published.

[18] D. B. Rawat and A. Alshaikhi, "Leveraging distributed blockchain-based scheme for wireless network virtualization with security and QoS constraints," in *Proc. International Conference on Computing, Networking and Communications, 2018*, pp. 332-336.

[19] E. Münsing, J. Mather, and S. Moura, "Blockchains for decentralized optimization of energy resources in microgrid networks," in *Proc. IEEE Conference on Control Technology and Applications, 2017*, pp. 2164-2171.

[20] K. Kotobi and S. G. Bilen, "Secure blockchains for dynamic spectrum access: A decentralized database in moving cognitive radio networks enhances security and user access," *IEEE Veh. Technol. Mag.*, vol. 13, no. 1, pp. 32-39, Mar. 2018.

[21] V. Buterin, "Ethereum White Paper: A Next-Generation Smart Contract and Decentralized Application Platform," 2013. [Online]. Available: https://github.com/ethereum/wiki/wiki/White-Paper

[22] N. Szabo. "Formalizing and securing relationships on public networks," *First Monday*, vol. 2, no. 9, 1997.

[23] V. Buterin, "On Public and Private Blockchains," 2015. [Online]. Available: https://blog.ethereum.org/2015/08/07/on-public-and-private-blockchains/

[24] Bitcoin forum, "Topic: Proof of stake instead of proof of work," 2011. [Online]. Available: https://bitcointalk.org/index.php?topic=27787.0

[25] M. Vukoli, "Rethinking Permissioned Blockchains," in *ACM Workshop on Blockchain, Cryptocurrencies and Contracts*, 2017, pp. 37.

[26] M. Castro and B. Liskov, "Practical Byzantine fault tolerance," in *Proceedings of the Third Symposium on Operating Systems Design and Implementation*, New Orleans, LA, 1999, pp. 173-186.
[27] C. Cachin, "Architecture of the hyperledger blockchain fabric," in *Proceedings of ACM Workshop on Distributed Cryptocurrencies and Consensus Ledgers*, Chicago, 2016.
[28] D. Ongaro and J. K. Ousterhout, "In search of an understandable consensus algorithm," in *Proceedings of 2014 USENIX Annual Technical Conference, Philadelphia*, PA, 2014, pp. 305-319.
[29] Quorum, "Quorum Whitepaper," 2016. [Online]. Available: https://github.com/jpmorganchase/quorum
[30] R. G. Brown, "The Corda platform: An introduction," 2018. [Online]. Available: https://www.corda.net/content/corda-platform-whitepaper.pdf
[31] T. T. A. Dinh, J. Wang, G. Chen, L. Rui, K. L. Tan, and B. C. Ooi, "BLOCKBENCH: A benchmarking framework for analyzing private blockchains," in *Proc. ACM SIGMOD Int. Conf. Manag. Data*, 2017, pp. 10851100.
[32] F. Baccelli and B. Blaszczyszyn, *Stochastic Geometry and Wireless Networks, Volume I-Theory*. NoW Publishers, 2009.
[33] R. Serfozo, *Introduction to stochastic networks*. Springer Science & Business Media, 2012.
[34] J. G. Andrews, F. Baccelli, and R. K. Ganti, "A tractable approach to coverage and rate in cellular networks," *IEEE Trans. Commun.*, vol. 59, no. 11, pp. 3122-3134, Nov. 2011.
[35] H. S. Dhillon, R. K. Ganti, F. Baccelli, and J. G. Andrews, "Modeling and analysis of K-tier downlink heterogeneous cellular networks," *IEEE J. Sel. Areas Commun.*, vol. 30, no. 3, pp. 550-560, Apr. 2012.
[36] J. G. D. Forney and G. Ungerboeck, "Modulation and coding for linear Gaussian channels," *IEEE Trans. Inf. Theory*, vol. 44, no. 6, pp. 2384-2415, Oct. 1998.
[37] M. Abramowitz and I. A. Stegun, *Handbook of Mathematical Functions with Formulas, Graphs, and Mathematical Tables*. New York, NY, USA: Dover, 1972.
[38] J. S. Ball, "Half-range generalized Hermite polynomials and the related Gaussian quadratures," *SIAM J. Numer. Anal.*, vol. 40, no. 6, pp. 2311-2317, 2002.
[39] N. M. Steen, G. D. Byrne, and E. M. Gelbard, "Gaussian quadratures for the integrals $\int_0^\infty e^{-x^2} f(x)\,dx$ and $\int_0^b e^{-x^2} f(x)\,dx$," *Math. Comput.*, vol. 23, no. 107, pp. 661-671, 1969.
[40] S. Boyd and L. Vandenberghe, *Convex Optimization*. Cambridge, U.K.: Cambridge Univ. Press, 2004.
[41] S. Boyd, N. Parikh, E. Chu, B. Peleato, and J. Eckstein, "Distributed optimization and statistical learning via the alternating direction method of multipliers," *Found. Trends in Mach. Learn.*, vol. 3, no. 1, pp. 1-122, Jan. 2011.
[42] E. Chen and M. Tao, "ADMM-based fast algorithm for multi-group multicast beamforming in large-scale wireless systems," *IEEE Trans. Commun.*, vol. 65, no. 6, pp. 2685-2698, Jun. 2017.
[43] J. Duchi, S. Shalev-Shwartz, Y. Singer, and T. Chandra, "Efficient projections onto the l_1-ball for learning in high dimensions," in *Proc. International Conference on Machine Learning, 2008*.
[44] R. M. Corless, G. H. Gonnet, D. E. G. Hare, D. J. Jeffrey, and D. E. Knuth, "On the Lambert W function," *Adv. Comput. Math.*, vol. 5, pp. 329-359, 1996.
[45] 3GPP TR 36.931, "LTE; evolved universal terrestrial radio access (E-UTRA); radio frequency (RF) requirements for LTE pico Node B," May 2011.